Absorption spectra of $Y_3Fe_5O_{12}$ (YIG) and $Y_3Ga_5O_{12}:Fe^{3+}$

G. B. Scott, D. E. Lacklison, and J. L. Page
Mullard Research Laboratories, Redhill, Surrey, England
(Received 29 October 1973)

The absorption spectra of $Y_3Fe_xGa_{5-x}O_{12}$ ($x = 5$, 3.9, 0.29, 0.09) at 300, 77, and 4.2 K have been recorded and least-squares fits to the spectra have been employed using a series of Gaussians whose energies, widths, and heights were adjustable parameters. This allowed a separation of overlapping contributions to the spectra arising from (i) crystal-field transitions with typical oscillator strengths of 10^{-5} and (ii) more broad intense bands occurring above 20 000 cm^{-1} with typical oscillator strengths of 10^{-3}. The crystal-field band energies were fitted using the cubic crystal-field matrices of Tanabe and Sugano. The oscillator strengths of bands of types (i) and (ii) which were resolved in both dilute and concentrated samples were found to be dependent on Fe^{3+} concentration implying Fe^{3+} pair interaction. This is consistent with type-(i) transitions being exciton-magnon bands; type-(ii) transitions may be double-exciton bands. A series of antiresonancelike lines observed in YIG at 4.2 K appear to be magnon and phonon sidebands of ${}^6A_{1g}({}^6S) \rightarrow {}^4E_g({}^4G)$ and ${}^6A_1({}^6S) \rightarrow {}^4E({}^4G)$ transitions.

I. INTRODUCTION

The absorption spectrum of the Fe^{3+} (d^5) ion is relatively little investigated compared with the other transition elements, particularly in comparison with the isoelectronic Mn^{2+} ion.[1,2] This is partly due to the ease with which Fe^{3+} forms covalent bonds with its ligands in a crystal (Fe^{3+} is rather more polarizable than Mn^{2+}) giving rise to charge-transfer transitions between the molecular-orbital levels of the Fe^{3+} ion and the ligands at energies which often obscure all but the lowest crystal-field transitions. The position of the ligand in the nephelauxetic series[3] is also an important factor in determining the degree of covalency and consequent energies of charge-transfer transitions between ligand and metal ion. This is clearly demonstrated by a comparison of the visible absorption spectra of FeF_3 (Ref. 4) and any of the ferric-oxide compounds ($Y_3Fe_5O_{12}$, this work; $YFeO_3$, Ref. 5).

The single-ion or single-molecular-complex picture is strictly applicable to dilute systems. In the concentrated magnetic compounds, inclusion of exchange and direct Coulomb interactions causes the excited states to be $\vec{k}$ dependent; i.e., the magnetic and electronic excitations are described by their respective band structures. Mattheiss[6] has shown that in the oxides of iron, cobalt, and nickel, covalency and overlap between the d states and the oxygen $2p$ states gives typical d bandwidths of 2.7 eV and produces a crystal-field-type splitting of the d bands in a similar manner to the splitting of the e and t_2 d levels in molecular-orbital theory.[7] In addition, it has been demonstrated that this overlap and covalency also raises the metal s and p conduction bands to higher energies.[6] Hence the absence of the low-mass s and p electrons reduces the screening between d electrons and a situation can exist where the Coulomb interaction energy exceeds the bandwidth. This results in localization of the d electrons producing high resistivity and the observation of single-ion phenomena, e.g., crystal-field-like transitions between the levels of these localized states.

Wemple[8] has recently reported absorption and reflectivity data for several iron garnets to around 6 eV and analyzed them in terms of contributions from the different types of transitions possible in this band picture. He identified (a) crystal-field transitions, (b) transitions from the oxygen $2p$ band to exciton levels below the $3d$ iron band, (c) transitions from the oxygen $2p$ band into $3d$ Bloch states (the d bands), and (d) transitions from the oxygen $2p$ band into the iron $4s$ band. Wemple[8] has not attempted any detailed assignments in these four regimes; this work is mainly concerned with an analysis of the crystal-field transitions and transitions of type (b) whose origin is discussed.

Early absorption measurements on YIG, mainly at 300 K, were limited by available sample thicknesses to energies below 20 000 cm^{-1}.[9-11] Wood and Remeika extended the energy coverage of study of Fe^{3+} absorption in the garnet structure by investigating samples of yttrium gallium garnet doped with Fe^{3+}.[11] By using the transition energies observed in the dilute and concentrated samples and assuming that all observed transitions were crystal field in origin, these authors[11] performed a crystal-field fit to these energies. As will be shown, dilution of the Fe^{3+} ion in YIG with Ga causes shifts in transition energies, and there are several transitions in this region of the spectrum which are not crystal-field transitions. Owing to these shifts in energy of the many closely spaced crystal-field levels originating from both tetrahedrally and octahedrally coordinated Fe^{3+}, and the

overlapping contributions of strong pair transitions, this method of crystal-field fitting must be treated with some caution. Blazey[12] has found difficulty in fitting his modulated reflectivity data for YIG to the Wood and Remeika energy scheme.[11]

Recently many iron garnets have been grown by epitaxy as single-crystal thin films of high optical quality[13] and some spectra reported.[8] However, there is evidence that films grown by the two standard techniques, chemical vapor deposition (CVD) and liquid-phase epitaxy (LPE) from lead based fluxes, suffer deviation from stoichiometry[14] and contain lead,[15] respectively. The CVD films tend to be Fe^{3+} deficient with an excess of Y^{3+} on both tetrahedral and octahedral sites.[14] Realizable levels of excess Y^{3+} will, to first order, only cause broadening of Fe^{3+} crystal-field transitions and lower the absorption level. The presence of Pb^{2+} in YIG, however, increases the absorption in the visible,[15] the origin of which increase has four possible sources: (i) s^2-sp Pb^{2+} transitions, (ii) photon-promoted electron hopping between Fe^{3+} and Fe^{4+} ions which are created to charge compensate the Pb^{2+}, (iii) charge-transfer transitions between Pb^{2+} and the anions, and (iv) Fe^{4+} absorption. In this case, the intrinsic spectrum of YIG is complicated by the presence of additional transitions, rendering assignments to Fe^{3+} transitions more difficult. For these reasons, we have chosen to record spectra of YIG from various sources putting most reliance on results obtained from thin sections of bulk material.

Reflectivity measurements on YIG have been reported by Grant,[16] on whose data a Kramers-Kronig analysis has been performed yielding the absorption spectrum of YIG to around 7 eV (56 000 cm^{-1}).[17] However, this analysis only exhibits significant structure above 2.8 eV (22 000 cm^{-1}), which has been assigned, although not in detail, to charge-transfer transitions between the molecular-orbital levels of Fe^{3+} and O^{2-}.[17] In particular, below 25 000 cm^{-1}, where reflectivity measurements are difficult to perform owing to a rapidly decreasing extinction coefficient, there is a region where, given samples of thickness around 1 μm, transmission spectra may be recorded. Wemple[8] has done this at 300 K and less detailed measurements have also been reported recently[18,19] at lower temperatures. By the combined procedures of recording the low-temperature spectra of YIG and the dilute garnets, Gaussian fitting and crystal-field fitting, we are able to make fairly confident, detailed assignments of most of the observed bands.

An interpretation of the YIG spectrum around 25 000 cm^{-1} is currently of interest as a result of the discovery of a large contribution to the Faraday spectrum of YIG and other iron garnets, induced by the presence of Bi^{3+}.[20–22] The transition or transitions responsible for this additional Faraday rotation lie in the 25 000-cm^{-1} region and as a first step in the understanding of the mechanism responsible, it is useful to assign an origin to transitions at these energies.

II. EXPERIMENTAL

YIG spectra were recorded using the following samples: (a) slices cut from single crystals grown from PbO/PbF_2 fluxes, (b) slices of polycrystalline YIG (Transtech G113), and (c) films rf sputtered onto $Gd_3Ga_5O_{12}$; spectra were recorded before and after annealing the films in oxygen.

This approach was adopted to ensure that there were no large impurity contributions to the spectra. Samples of $Y_3Fe_xGa_{5-x}O_{12}$ ($x = 3.85, 0.29, 0.09$) were obtained from crystals grown from PbO/PbF_2 fluxes. The major impurities found in these materials by mass-spectrographic analysis are summarized in Table I.

Sample thicknesses down to 1.5 μm were obtained by Syton polishing; sample thicknesses to 0.5 μm were obtained by ion-beam milling thin sections prepared by polishing. All samples were used free standing over apertures.

Absolute determination of absorption coefficient requires a knowledge of sample thickness and reflectivity. Thicknesses greater than 10 μm were determined by a commercial electromechanical instrument, less than 10 μm using interference oscillations. Comparison of the periodicity of the oscillations for samples of different thicknesses allowed a determination of the refractive index which is summarized in Table II for YIG. There is good agreement with the data of Johnson and Walton[23] in the region of overlapping wavelength. The refractive index of YIG determined by Kahn *et al.*[17] from Grant's reflectivity data[16] are consistently lower than our values. This is in keeping with Wemple's assertion[8] that the reflectivity of YIG determined by Grant[16] is too low.

The 300-K and 77-K spectra were recorded on a Hitachi EPS 3T double-beam spectrophotometer. The 4.2-K YIG spectrum was recorded using a

TABLE I. Major impurity concentrations in samples studied.

Nominal composition	Impurity (ppm atomic)						
	Pb	Si	Ni	Zn	Ca	Mg	Mn
$Y_3Fe_5O_{12}$ (flux grown)	320	50	<2	<1	<8	12	12
$Y_3Fe_5O_{12}$ (G113)	<1	1100	43	45	470	330	220
$Y_3Fe_{3.85}Ga_{1.15}O_{12}$	270	250	<1	<1	6	<10	<1
$Y_3Ga_5O_{12}$	170	90	<1	<1	35	<3	<1
$Y_3Fe_{0.09}Ga_{4.91}O_{12}$	130	atomic absorption test for Pb only					
$Y_3Ge_{0.29}Ga_{4.71}O_{12}$	150						

TABLE II. Refractive index of YIG from interference oscillations (n_{osc}) compared with values from Johnson and Walton, Ref. 23 (n_{JW}).

Wavelength (nm)	n_{osc}	n_{JW}
550	2.34	
650	2.27	
750	2.24	
850	2.23	
950	2.20	
1100	2.19	
1400	2.18	2.209
1600	2.16	2.200
1800	2.15	2.194
2000	2.14	2.188
2500	2.13	2.177

McPherson spectrophotometer fitted with an Oxford Instruments continuous flow cryostat. The absorption spectra of YIG and $Y_3Fe_xGa_{5-x}O_{12}$ ($x = 0.29, 0.09$) were corrected for reflection loss using functions fitted to the data of Tables II and III.

III. SPECTRA $Y_3Fe_5O_{12}$

Figure 1 shows the absorption spectrum from 10 000 to around 25 000 cm^{-1}. The low-energy end is not reproduced here for 300 K as it has been presented before[8–11]; this part of the spectrum was recorded at 77 K using samples of single-crystal slices cut from bulk material. Above 20 000 cm^{-1}, spectra were recorded using single-crystal, polycrystalline, and rf-sputtered material but only the polycrystalline spectrum is shown in Fig. 1.

The differences in the spectra of the YIG from the various sources are now discussed.

The absorption spectra of rf-sputtered films prior to annealing exhibited higher absorption than after annealing. Typical increases in transmission were from 8 to 50% around 20 000 cm^{-1} for films 0.5 μm thick. No spectral features were discernible in the films prior to annealing apart from a steadily increasing absorption level as higher energy was approached. The spectra recorded on annealed films, single-crystal slices, and polycrystalline slices were very similar; the pertinent differences were as follows: (i) bandwidths for the better resolved transitions at 20 700, 21 390, and 22 530 cm^{-1} were identical in polycrystalline and single-crystal slice samples; (ii) the absorption coefficients above 20 000 cm^{-1} were on the average 8% higher for single-crystal slices than for polycrystalline samples. We have not made a comparison at lower energies; (iii) bandwidths for transitions at 20 700, 21 390, and 22 530 cm^{-1} were typically 80% greater in the annealed films than in single-crystal and polycrystalline slices.

The probable effects of the presence of Pb^{2+} on the YIG spectra may be obtained from a knowledge of the spectrum of $Y_3Ga_5O_{12}$ grown from PbO/PbF_2 fluxes. Figure 2 shows the spectrum of a sample of $Y_3Ga_5O_{12}$ containing 170 ppm atomic of Pb^{2+} (i.e., $Y_{2.996}Pb_{0.004}Ga_5O_{12}$). The band at 35 900 cm^{-1}, probably the Pb^{2+} $^1S_0 \rightarrow {}^3P_1$ transition, has an oscillator strength of 0.05; there is a shoulder at 43 000 cm^{-1} ($^1S_0 \rightarrow {}^3P_2$) but the oscillator strength is difficult to estimate owing to the strong edge at 45 000 cm^{-1}. This spectrum is very similar to that found for $Y_3Ga_5O_{12}$:Bi^{3+} (Ref. 24) (Bi^{3+} is isoelectronic with Pb^{2+}). From the known concentration of Pb^{2+} in the polycrystalline and single-crystal samples these Pb^{2+} bands would only contribute features of magnitude < 2 and 696 cm^{-1}, respectively, at 35 900 cm^{-1}. The additional absorption in the single-crystal samples for energies above 20 000 cm^{-1} is tentatively attributed to the presence of Fe^{4+}, which charge compensates for Pb^{2+}. Additional support for this view is lent by the observation that YIG films grown by liquid-phase epitaxy with PbO/PbF_2 fluxes have absorption levels in the visible and near infrared well above similar films free of lead.[15]

The two major features of the YIG spectrum are the existence of a series of closely spaced weak transitions starting around 11 000 cm^{-1} superimposed on a region of much stronger absorption which begins around 21 000 cm^{-1}. The change of slope at 21 930 cm^{-1}, the strong transition at 23 260 cm^{-1}, and a continuously rising edge above 24 000 cm^{-1} appear to suggest that there are a few strong transitions present in this region which dominate the spectrum. Some of the weaker transitions have considerable width; the band centered at 11 070 cm^{-1} has a full width at half-height (2Γ) of 2000 cm^{-1}. However, all these bands are multicomponent, an example of which is shown in Fig. 3 for the band at 11 070 cm^{-1}. The resolution of three narrower transitions at 20 700, 21 390, and 22 530 cm^{-1} at 77 K is noteworthy for their importance in the analysis that follows. Figure 4 shows a portion of the spectrum at 4.2 K between 20 000 and

TABLE III. Refractive index of $Y_3Ga_5O_{12}$ obtained by minimum angle of deviation on a polished prism.

Wavelength (nm)	$n \pm 0.003$
425	1.948
450	1.937
475	1.934
500	1.935
525	1.930
550	1.921
600	1.916
625	1.910
650	1.908
675	1.905
700	1.904

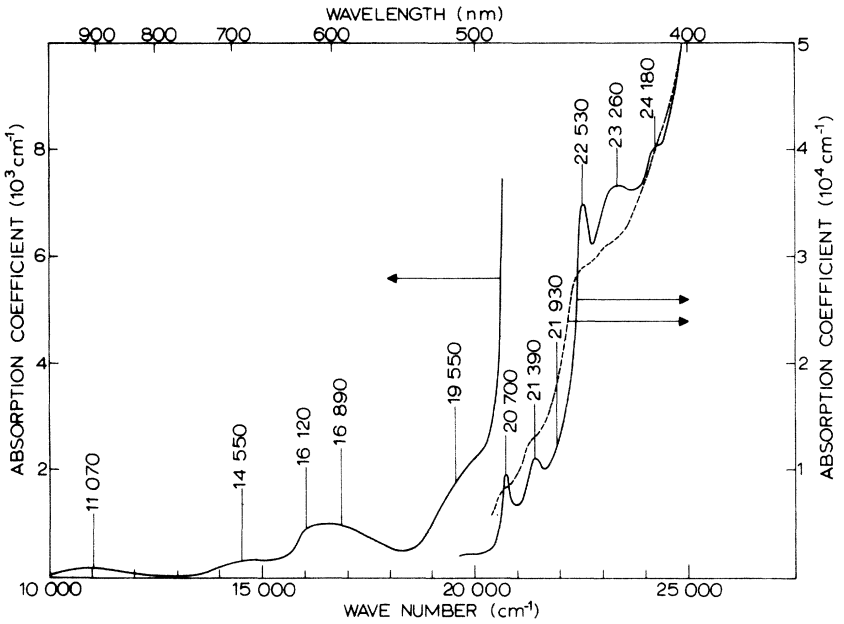

FIG. 1. Absorption spectrum of $Y_3Fe_5O_{12}$ at 77 K (solid line) and 300 K (dashed line) (corrected for reflection loss).

22 500 cm^{-1}, demonstrating that the well resolved bands at 20 700 and 21 450 cm^{-1} are split with components at 20 970 and 21 320 cm^{-1}, respectively. In addition, there is weak structure at the energies listed in Table V; the most easily discernible of this detail is shown in Fig. 5. The form of this structure is not that of a normal absorption peak but bears more resemblance to weak inverted absorption bands superimposed on the broad background absorption. Such phenomena have been previously reported[25,26] when the sharp line of an impurity overlapped a broad vibronic band giving rise to line shapes similar to those of Fig. 5. Possible sources of these antiresonancelike lines are given in the ensuing discussion.

A. $Y_3Ga_{1.15}Fe_{3.85}O_{12}$

The 77-K spectrum of flux-grown crystals, shown in Fig. 6, reveals that at all energies, the absorption level is lower than YIG. Gallium has a tetrahedral-site preference in YIG, and in $Y_3Ga_{1.15}Fe_{3.85}O_{12}$ more than 80% of Ga^{3+} ions will occupy tetrahedral sites.[27] Consequently, one might expect a reduction in strength only of transitions associated with tetrahedral Fe^{3+}. That *all* transition intensities are reduced is in agreement with Wemple's[8] report that preferential dilution of *either* tetrahedral or octahedral Fe^{3+} reduces the strength of *all* transitions. Discussion of these phenomena is reserved for Sec. VII.

The other feature of the spectrum of $Y_3Fe_{3.85}Ga_{1.15}O_{12}$ is the considerable broadening of all transitions even at 77 K. These transitions are much better resolved in both YIG and $Y_3Ga_5O_{12}$ containing small levels of Fe^{3+}. In these two materials, Fe^{3+} ions exist in fixed coordination with nearest-neighbor cations. In $Y_3Fe_{3.85}Ga_{1.15}O_{12}$, there are many nearest-neighbor cation coordina-

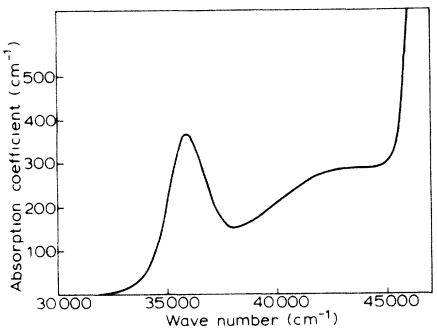

FIG. 2. Absorption spectrum of $Y_3Ga_5O_{12}$: Pb^{2+} at 300 K; Pb^{2+} concentration at 170 ppm atomic.

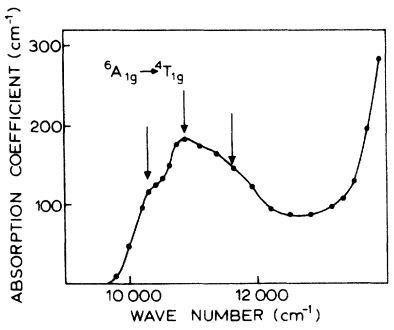

FIG. 3. Detail of $^6A_{1g}(^6S) \rightarrow {}^4T_{1g}(^4G)$ in $Y_3Fe_5O_{12}$ at 77 K, showing three major components.

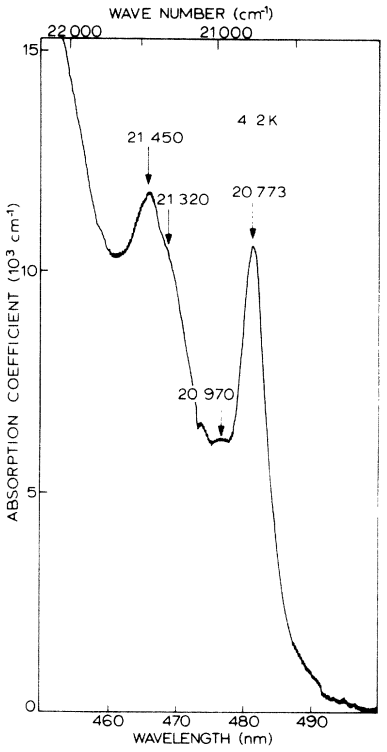

FIG. 4. Detail of $Y_3Fe_5O_{12}$ spectrum between 20 000 and 25 000 cm^{-1}, showing splitting (arrowed) of $^6A_{1g}(^6S) \rightarrow {}^4E_g$; $^4A_{1g}(^4G)$ and $^6A_1(^6S) \rightarrow {}^4E$; $^4A_1(^4G)$.

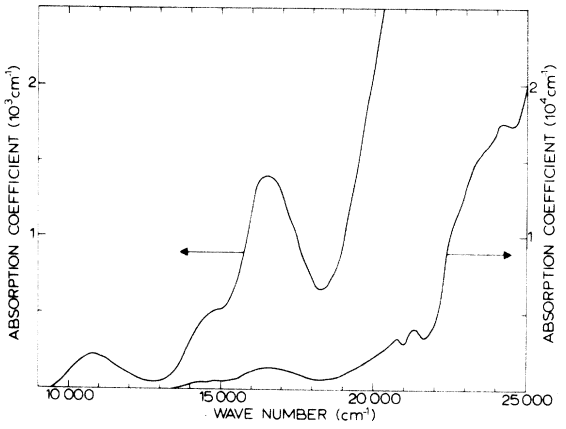

FIG. 6. Absorption spectrum of $Y_3Ga_{1.15}Fe_{3.85}O_{12}$ at 77 K (corrected for reflection loss).

features of the spectra are the reduction in intensity of the weaker crystal-field-like transitions with respect to the region of high absorption above 20 000 cm^{-1} and the two sharp lines at 23 950 and 24 380 cm^{-1}, particularly at 77 K in the more-dilute garnet. Again the spectra consists of a series of closely spaced transitions, being particularly complex around 26 000 cm^{-1}. However, using the re-

tions for Fe^{3+}, each of which causes small shifts of the energy of the Fe^{3+} transitions.

B. $Y_3Fe_xGa_{5-x}O_{12}$ ($x = 0.09, 0.29$)

Figures 7 and 8 show the room-temperature and 77-K spectra of $Y_3Fe_{0.09}Ga_{4.91}O_{12}$ and $Y_3Fe_{0.29}Ga_{4.71}O_{12}$, respectively. The most striking

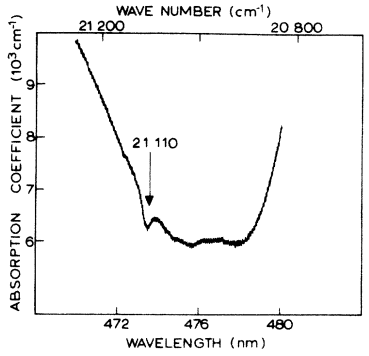

FIG. 5. Detail of antiresonancelike lines at 21 110 cm^{-1} in YIG.

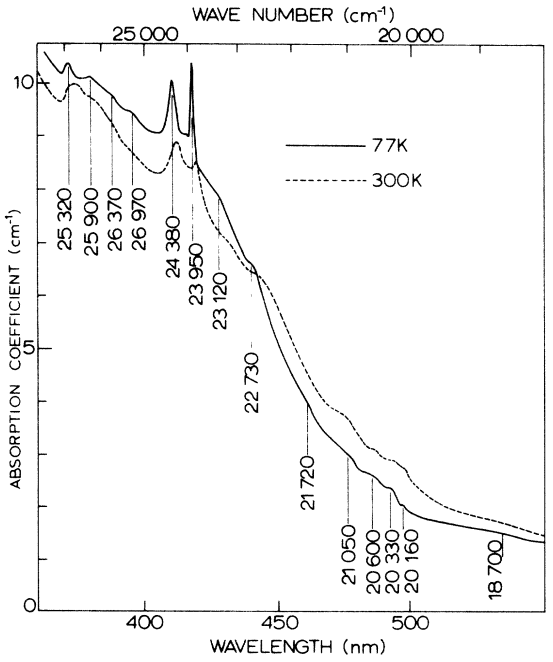

FIG. 7. Absorption spectrum of $Y_3Fe_{0.09}Ga_{4.91}O_{12}$ at 300 and 77 K.

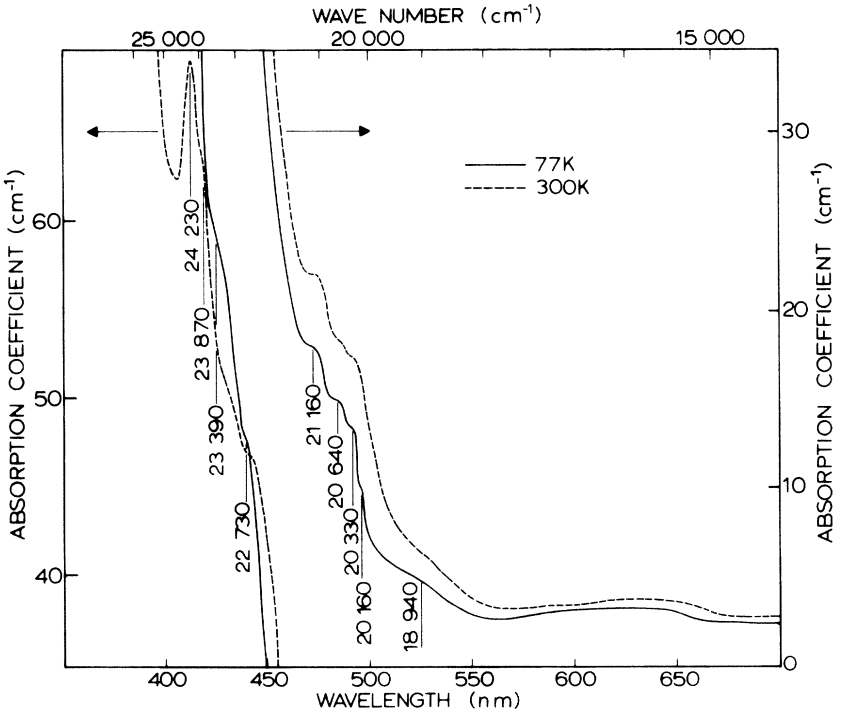

FIG. 8. Absorption spectrum of $Y_3Fe_{0.29}Ga_{4.71}O_{12}$ at 300 and 77 K.

sults of the Gaussian fitting and the crystal-field analysis, crystal-field transitions may be identified in the higher-energy regions of these spectra. The absorption bands below 18 000 and 14 000 cm^{-1} in $Y_3Fe_{0.09}Ga_{4.91}O_{12}$ and $Y_3Fe_{0.29}Ga_{4.71}O_{12}$, respectively, are not shown as they were very weak. Their energies were determined using a composite sample formed by butting together the polished faces of several crystals. Also not shown in Figs. 7 and 8 is a strong absorption band at 29 000 cm^{-1} which was observed in $Y_3Fe_{0.09}Ga_{4.91}O_{12}$.

IV. GAUSSIAN FITTING

From previous analyses of the YIG spectrum,[9-11] the origin of the region below about 20 000 cm^{-1} is understood. However, there are six transitions (many more if splittings and fine structure are included) between 20 000 and 25 000 cm^{-1} compared with only four between 10 000 and 20 000 cm^{-1}. It was not clear whether these overlapping transitions occurring above 20 000 cm^{-1} were weak transitions sitting on a rapidly rising edge or if several of these transitions were of such a magnitude as to contribute significantly to the absorption. As an aid to interpretation in this region use was made of a computer program which fitted a series of Gaussians to the spectrum by a least-squares method, minimizing the error function with respect to Gaussian height, width, and position (energy). Data points were taken from the absorption trace and run with an initial set of Gaussian parameters which were estimated by inspection of the absorption traces. The energy, width, and height of the transition producing the edge above 30 000 cm^{-1} (Fig. 1) was estimated from the Fe^{3+}-doped $Y_3Ga_5O_{12}$ spectra. The results of the Gaussian fitting are shown in Fig. 9, where the fit to the data points is presented with the Gaussian components used to produce the fit. A plot, versus wave num-

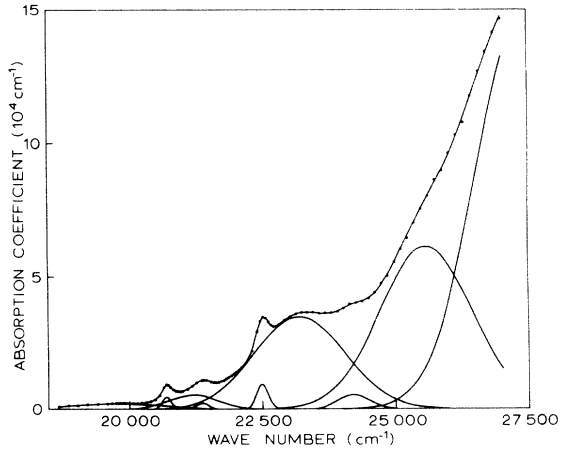

FIG. 9. Gaussian least-squares fit (full curve) to absorption spectrum of YIG (data points) showing Gaussian components which gave the fit.

ber, of the squares of the deviations between data values and fitted values showed that fitting was always comparable with the experimental error inherent in the data. We are aware that the Gaussian spectrum resulting from the fit does not necessarily represent the exact magnitude of the contributions from each transition present in YIG but we believe it does represent a useful approximation. This is borne out by the consistency with which transitions shown to be weak from Gaussian fitting fit well into an energy scheme for crystal-field transitions in YIG and Fe^{3+}-doped $Y_3Ga_5O_{12}$. Figure 9 shows that the major contributions to the YIG spectrum between 20 000 cm and 28 000 cm^{-1} arise from transitions at 23 110, 25 600, and 27 400 cm^{-1}, the edge of the latter being shown in Fig. 9. The very low wide Gaussian just below 20 000 cm^{-1} was used to fit the envelope produced by three overlapping components which were only resolved at 4.2 K. In the initial estimate of transition energies produced as input to the minimization program, a peak was given at 22 000 cm^{-1} which corresponds to the region exhibiting a sudden change in slope. The fitting required that this peak be shifted to lower energy at 21 640 cm^{-1}; all other fitted energies were very close to the initial estimates. At 21 720 cm^{-1} in the spectrum of $Y_3Fe_{0.09}Ga_{4.91}O_{12}$ (Fig. 7) there is a shoulder and this, in conjunction with Wemple's data,[8] indicates that a band is indeed present at 21 640 cm^{-1} in YIG. The data to 25 000 cm^{-1} was taken from polycrystalline G113 YIG and from 25 000 to 28 000 cm^{-1} from an rf-sputtered film, hence the highest energy data may not be as reliable as the rest. However, the transition at 27 400 cm^{-1}, the tail of which is seen in the fit, has been observed by Blazey,[12] Wemple,[8] and Wittekoek (private communication).

As a result of this fitting the transitions at 20 700, 21 390, 22 530, and 24 180 cm^{-1} are seen to be generally narrower and weaker than the other transitions and, therefore, we include these with the transitions below 20 000 cm^{-1} in the crystal-field fit. For the dilute iron garnets a series of 15 peaks was used to fit the data between 17 500 and 27 500 cm^{-1} with initial estimates of width, height, and position of band maxima being taken directly from the traces. The results of the fit to the 77-K spectrum of $Y_3Fe_{0.09}Ga_{4.91}O_{12}$ is shown in Fig. 10, where it can be seen that the three strong transitions at 23 440, 25 650, and 29 120 cm^{-1} dominate the spectrum. Owing to their large width, these peaks are not well defined by the experimental spectrum and consequently their computed widths and heights are more susceptible to error than those of the better resolved transitions. However, this general approach is again vindicated by the parallel observation by Wemple[8] of strong transitions at 23 500, 25 400, and 29 500 cm^{-1} in $Y_3Fe_{0.31}Ga_{4.69}O_{12}$. From their larger width and strength we preclude the possibility of the transitions occurring at the following energies from being crystal field in origin: 21 640, 23 440, 25 648, 26 320, 27 400, and 29 120 cm^{-1}. The remaining transitions we attempt to fit into a crystal-field scheme. The reason that we do not observe the transition at 27 400 cm^{-1} which is seen in YIG is discussed in Sec. VII.

Although not shown here, Gaussian fits to the spectra of $Y_3Fe_{3.85}Ga_{1.15}O_{12}$ and $Y_3Ga_{4.71}Fe_{0.29}O_{12}$ were performed with similar results to those obtained with YIG and $Y_3Fe_{0.09}Ga_{4.91}O_{12}$. Table IV lists the energies of the transitions observed in the dilute materials at 77 K and lists for comparison those given by Wemple[8] for $Y_3Ga_{4.69}Fe_{0.31}O_{12}$ at 300 K. Where a band was not clearly resolved in the experimental spectrum its energy was taken from the Gaussian fit and its entry in Table IV is preceded by a G. Table V lists the transition energies observed in YIG at 77 and 4.2 K by us and by Blazey[12] using modulated reflectivity at 77 K. Blazey did not list these energies,[12] which we obtained from his data making the following assumptions. If R is the complex reflectivity of a material for normal incidence then the real part of $\Delta R/R$ is given by

$$\mathrm{Re}\left(\frac{\Delta R}{R}\right) = \frac{4(n^2-k^2-1)\,\Delta n + 8nk\,\Delta k}{[(n+1)^2+k^2][(n-1)^2+k^2]} = A\Delta n + B\Delta k\,, \tag{1}$$

where n and k refer to the real and imaginary parts

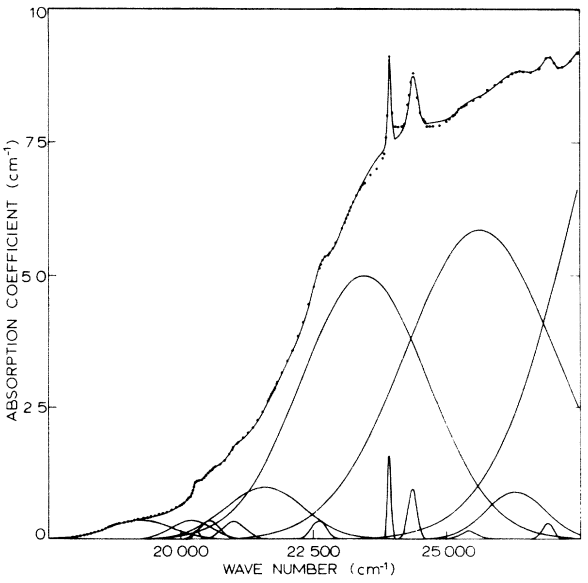

FIG. 10. Gaussian fit to the absorption spectrum of $Y_3Fe_{0.09}Ga_{4.91}O_{12}$ at 77 K.

TABLE IV. Comparison of transition energies (cm^{-1}) in $Y_3Fe_{0.31}Ga_{4.69}O_{12}$ (300 K), Ref. 8, with those in $Y_3Fe_{0.29}Ga_{4.71}O_{12}$ and $Y_3Fe_{0.09}Ga_{4.91}O_{12}$ (77 K). The letter *G* denotes that the energy was obtained by Gaussian fitting.

$Y_3Fe_{0.31}Ga_{4.69}O_{12}$ (Ref. 8)	$Y_3Fe_{0.29}Ga_{4.71}O_{12}$	$Y_3Fe_{0.09}Ga_{4.91}O_{12}$
11 130	10 640	10 300
14 275	14 290	13 800
15 970	16 340	15 400
19 250	19 380	18 730
19 842	20 160	20 160
20 245	20 330	20 330
20 568	20 640	20 600
21 052	21 160	21 050
21 616 } 22 181 }		21 640 *G*
22 504	22 730	22 730
23 230	23 390	23 440 *G*
23 875	23 870	23 950
24 198	24 230	24 380
25 490		25 460 *G*
25 810		25 650 *G*
26 130		26 320 *G*
26 700		26 970
		29 000

of the refractive index N. Using n and k for YIG,[8] the contribution to $\mathrm{Re}(\Delta R/R)$ at 3 eV from changes in the refractive index Δn are an order of magnitude greater than those from changes in the extinction coefficient Δk. Consequently, the line shapes of $\mathrm{Re}(\Delta R/R)$ are well described in YIG below 3 eV by

$$\frac{4(n^2-k^2-1)\,\Delta n}{[(n+1)^2+k^2][(n-1)^2+k^2]}\,, \tag{2}$$

which for $n \gg k$ reduces to the differential of a dispersive line shape, having a negative peak at the transition.

Clearly there is good agreement between the data obtained by the three techniques of modulated reflectivity,[12] modulated absorption,[8] and direct absorption. It is noteworthy that direct-absorption measurements at 4.2 K revealed more structure than the modulated-reflectivity method at 77 K[12] and the modulated-absorption technique at 300 K.[8] For the iron-doped yttrium gallium garnets agreement with Wemple's data[8] is generally good but there are noticeable differences in energy for transitions below 20 000 cm^{-1}. This is undoubtedly due to the fact that most of these bands are multicomponent and do not provide well defined band maxima except in very thick samples at low temperatures. Of the three types of YIG samples employed in recording spectra, the single-crystal, thin sections exhibited the highest level of absorption. However, this increased absorption level was only 8% above that of polycrystalline YIG. Since the spectral structure exhibited by all three sources of YIG was identical, we feel confident that there were no large impurity contributions to the spectrum and that our analysis in terms of Fe^{3+} transitions is valid.

V. CRYSTAL-FIELD ANALYSIS AND ASSIGNMENTS

We expect the optical spectrum of YIG to contain contributions from *d* states which are strongly localized and split by the crystal field produced by the ligands. In YIG, the Fe^{3+} ions occupy two sites as denoted in the YIG formula unit, $\{Y_3\}[Fe_2](Fe_3)O_{12}$; two Fe^{3+} ions are octahedrally coordinated with O^{2-} and three Fe^{3+} ions are tetrahedrally coordinated with O^{2-}. Yttrium iron garnet has the space group O_h^{10}-$Ia3d$ and the tetrahedral

TABLE V. Transition energies (cm^{-1}) observed in YIG at 77 and 4.2 K. The letter *G* denotes that the energy was obtained from Gaussian fitting and the letter *F* refers to the weak, fine structure. Bracketed energies are those which would be degenerate under O_h and T_d.

77 K	4.2 K	Ref. 11, 77 K
10 400 } 11 000 } 11 600 }		
14 550 *G*		
16 120 } *G* 16 890 } *G*	16 160 } 16 420 } 17 360 }	
	19 190 }	
19 718 *G*	19 650 } 20 200 }	
	20 346 *F*	
20 710	20 773 } 20 970 }	20 800
	21 110 *F*	
21 228 *G*		
21 390	21 320 } 21 450 }	21 400
	21 505 *F*	
	21 786 *F*	
	21 835 *F*	
	21 930 *F*	
	22 095 *F*	
	22 202 *F*	
22 520	22 550	22 500
23 110 *G*	23 280	23 200
	23 600	
24 150	24 200	24 200
25 600 *G*		
25 800		25 400
27 400 *G*		

and octahedral Fe^{3+} sites are distorted, having point groups $\bar{4}$ and $\bar{3}$, respectively.

Owing to the complexity of the YIG spectrum from contributions from two different symmetry sites we will analyze the contributions of tetrahedrally and octahedrally coordinated Fe^{3+} in terms of transitions between the set of d^5 states split by the crystalline fields of T_d and O_h symmetry, respectively.

The free-ion energy levels of the $3d^5$ configuration consist of a high-spin ground state, ^6S above which exist a series of spin quartet states, ^4G, ^4P, ^4D, ^4F, separated from ^6S by typically 30 000 cm^{-1}. These levels split in a cubic field as described by Orgel[28] (Fig. 11). The crystal-field strength Dq is generally at least twice as great for octahedrally coordinated ions as it is for tetrahedrally coordinated ions[2] and, therefore, the $^4T_{1g}(^4G)$ and $^4T_{2g}(^4G)$ states will occur at lower energies than the $^4T_1(^4G)$ and $^4T_2(^4G)$ levels. Transitions to these states should also be distinguishable on intensity grounds since the octahedral (or $\bar{3}$) symmetry causes transitions between $^6A_{1g}(^6S)$ and any of the ^4G manifold to be parity forbidden. The lack of inversion at the tetrahedral site allows static mixing of higher-energy, high-intensity, odd-parity transitions into the ground state relaxing the parity constraint. Consequently, transitions between the $^6A_1(^6S)$ ground state and the quartet excited states, being only spin forbidden, should exhibit higher intensity than those between

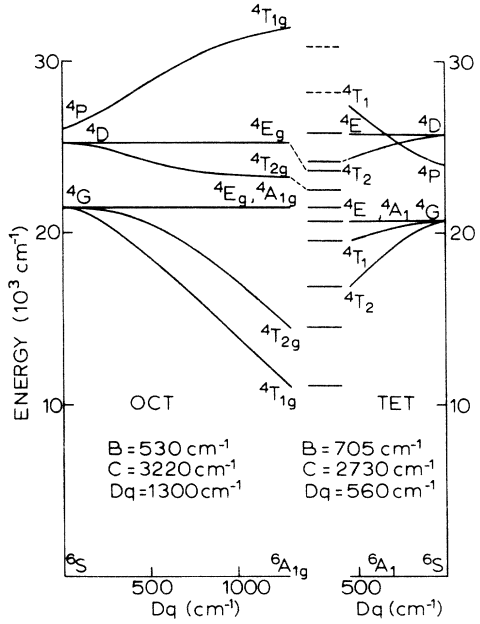

FIG. 11. Crystal-field fit to the absorption spectrum of tetrahedral and octahedral Fe^{3+} in $Y_3Fe_5O_{12}$ at 77 K.

$^6A_{1g}(^6S)$ and the excited quartet levels. Figure 9 shows that there is considerable overlap between some crystal-field transitions and the more intense bands and therefore these crystal-field transitions may borrow intensity. One must exhibit extreme caution in using intensity arguments in assigning transitions in these regions. However, no such overlap occurs for transitions below 20 000 cm^{-1}. Therefore, the fact that the transitions at 16 500 and 19 500 cm^{-1} are of considerably higher intensity than those at 11 000 and 14 550 cm^{-1} is in agreement with the fact that octahedral transitions occur at lower energies than the equivalent tetrahedral ones. In accordance with previous workers[8-10] we assign the bands at 11 000 and 14 550 cm^{-1} to $^6A_{1g}(^6S) \rightarrow {}^4T_{1g}(^4G)$ and $^6A_{1g}(^6S) \rightarrow {}^4T_{2g}(^4G)$; those at 16 500 and 19 500 cm^{-1} are assigned to the corresponding tetrahedral transitions.

It has been shown[29] that transitions between states of different orbital electronic configurations should be broad compared to those between states of the same orbital electronic configuration. Among the quartet levels, $^4E(^4G)$, $^4A_1(^4G)$, $^4E(^4D)$, and $^4A_2(^4F)$ have the same orbital configuration as the ground state, i.e., $t_2^3e^2$. We use this fact to assign the bands at 20 770 cm and 21 450 cm^{-1} to the transitions $^6A_{1(g)}(^6S) \rightarrow {}^4E_{(g)}$, $^4A_{1(g)}(^4G)$. Further support for this assignment is the observation at 4.2 K (Fig. 4) of components of these two bands which are weaker and separated by 200 and 130 cm^{-1}, respectively, from the 20 770 and 21 450 cm^{-1} peaks. The degeneracy of the $^4E, {}^4A_1(^4G)$ states is not removed under $\bar{3}$ or $\bar{4}$ symmetry but Koide and Pryce[30] considered the effects of covalency on these states for the $Mn^{2+}(3d^5)$ ion in octahedral coordination in MnF_2 and showed that the degeneracy would be lifted. In addition, they showed that the ^4E_g state lay above or below $^4A_{1g}$ depending on the degree of covalency, and concluded that in MnF_2, $^4A_{1g}$ lay below ^4E_g. Consequent experiments indicated that in fact the $^4A_{1g}$ level lay above ^4E_g. Lohr[31] reconsidered the problem of the order of the splitting, showing that the sign of the splitting was critically dependent on the degree of covalency experienced by the t_{2g} and e_g electrons. This was not the case for tetrahedral coordination, where the ^4E state would be below $^4A_1$.[31] The split ^4E_g and $^4A_{1g}$ states in MnF_2 (Ref. 32) and other manganese fluorides[33] consists of a sharp line with an adjacent broader band of lower intensity. The narrow line corresponds to $^6A_{1g}(^6S) \rightarrow {}^4E_g(^4G)$, the broader to $^6A_{1g}(^6S) \rightarrow {}^4A_{1g}(^4G)$. These states of the Fe^{3+} ion exhibit identical structure in octahedral coordination at low temperature, e.g., $Al_2O_3:Fe^{3+}$.[34] In YIG at 4.2 K (Fig. 4) we see similar behavior, two relatively sharp strong peaks at 20 770 and 21 21 450 cm^{-1} with broader, lower-intensity components at 20 970 and 21 320 cm^{-1}, respectively.

By analogy with the result for Mn^{2+},[31] we assign the lower-energy bands to tetrahedral Fe^{3+}, since for these the broader, $^4A_1$, state lies above the sharper stronger ^4E line. The transitions at 20 970 and 20 770 cm^{-1} are consequently ascribed to $^6A_{1g}(^6S) \rightarrow {}^4E_g(^4G)$ and $^6A_1(^6S) \rightarrow {}^4A_1(^4G)$, respectively.

Having now assigned the above transitions, we use their energies in conjunction with the energy matrices of Tanabe and Sugano[35] for d^5 ions in a cubic field, to obtain values for B, C, and Dq for both tetrahedral and octahedral Fe^{3+}. Using the calculated values of B, C, and Dq the energies of the higher states were evaluated and compared with experiment to aid further assignments.

This procedure was first carried out for YIG (77 K), but later for $Y_3Fe_{0.09}Ga_{4.91}O_{12}$ (77 K) to check that our assignments for the two materials were consistent. Figure 11 shows the results for YIG where the energies of the transitions, shown to be of low intensity by Gaussian fitting, are compared with the calculation. The agreement between calculation and experiment is fair and indicates that the transitions at 22 520 and 25 800 cm^{-1} correspond to $^6A_{1g}(^6S) \rightarrow {}^4T_{2g}(^4D)$ and $^6A_1(^6S) \rightarrow {}^4E(^4D)$, respectively; of necessity the calculated $^6A_1(^6S) \rightarrow {}^4T_1(^4G)$, $^4T_2(^4G)$, and ^4E; $^4A_1(^4G)$ energies must agree with experiment. The assignments made in Fig. 11 for the transitions at 24 150 and 23 600 cm^{-1} have been made to maintain consistency with the assignments made for $Y_3Fe_{0.09}Ga_{4.91}O_{12}$ at these energies, where more information on the origin of these transitions is available. It should be noted that if the assignments of $^6A_1(^6S) \rightarrow {}^4E$, $^4A_1(^4G)$ and $^6A_{1g}(^6S) \rightarrow {}^4E_g$, $^4A_{1g}(^4G)$ are reversed and the spectrum recalculated, an identical set of assignments best describes the experimental spectrum in YIG. It has recently been reported[18] that there also exist transitions in YIG at 30 800 (shoulder) and at 28 170 cm^{-1} (sharp line). Although these transition energies would agree fairly well with the calculated energies of $^6A_{1g}(^6S) \rightarrow {}^4T_{1g}(^4P)$ at 30 700 cm^{-1} and $^6A_1(^6S) \rightarrow {}^4T_1(^4P)$ at 29 500 cm^{-1}, we maintain some reservation concerning this result which was reported for epitaxial films, the thinnest of which was quoted as being 1 μm.[18] From the known absorption coefficient of YIG at these energies,[8] such a film would have an optical density of greater than 10 at 29 000 cm^{-1}. Since the spectrophotometer used,[18] a Cary 17R, can handle an optical density of 6 at most, this result must be treated with caution. We have measured the Faraday rotation of single-crystal and polycrystalline slices of YIG up to 25 000 cm^{-1} and obtained results which agree to within 3% for the magnitude of the peak at 22 990 cm^{-1}.[20] This value is 34 000 deg/cm, which is approximately three times greater than that quoted in Ref. 18. We suggest that the epitaxial film used in the above work[18] was nearer 0.3 μm in thickness, thus giving an optical density of around 3, which could be easily handled. For completeness, the energies of these reported transitions are included as dotted lines in Fig. 11.

The $^4T_2$ states are made up from the strong field configurations t_2^4e, $t_2^3e^2$, and $t_2^2e^3$, the second of which is the ground-state configuration. The relatively small dependence of the energy of $^4T_2(^4D)$ on Dq compared with $^4T_2(^4G)$ and $^4T_2(^4F)$ shows that this state contains a major contribution from $t_2^3e^2$ and consequently the $^6A_1(^6S) \rightarrow {}^4T_2(^4D)$ transitions appear sharper than the $^6A_1(^6S) \rightarrow {}^4T_2(^4G)$.

The ratio of Dq values for octahedral and tetrahedral Fe^{3+}, being 2.3, is close to the ratio expected for these coordinations.[2] The Racah parameter B is similar for both coordinations and is 58 and 76% of the free-ion value.[36] This reduction is more acceptable than some previously quoted values for Fe^{3+} in complexes[37] and is in reasonable agreement with values given in Ref. 1.

Figure 12 shows the result of the crystal-field calculation for $Y_3Fe_{0.09}Ga_{4.91}O_{12}$. The energy taken for the ^4E, $^4A_1(^4G)$ states, degenerate in a cubic field, was the mean of the two transitions at 20 160 and 20 330 cm^{-1}; similarly for the ^4E_g, $^4A_{1g}(^4G)$ energies the mean of 20 640 and 21 160 cm^{-1} was taken. This ordering is the same as used for YIG. The observation of weak, narrow, crystal-field-like transitions at higher energies in the dilute

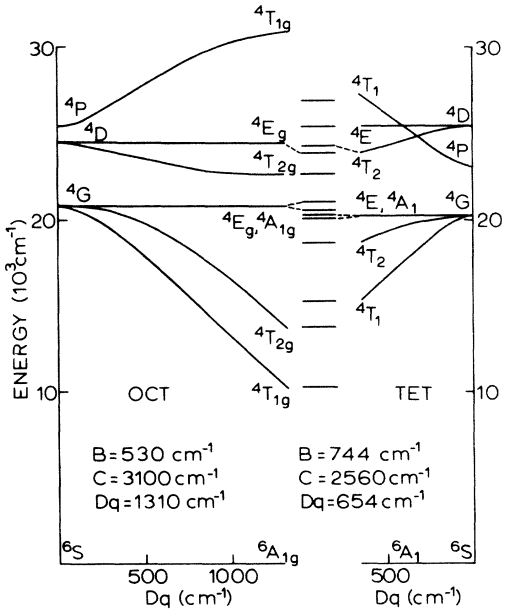

FIG. 12. Crystal-field fit to the absorption spectrum for tetrahedral and octahedral Fe^{3+} in $Y_3Fe_{0.09}Ga_{4.91}O_{12}$ at 77 K.

garnets allows a better comparison between experiment and calculation. The over-all correlation between calculated and experimentally observed transition energies is better for the dilute garnets than for YIG, as might be expected since the dilute iron garnets would give spectra which were more representative of single-Fe^{3+}-ion behavior. The reason for assigning the transition at 23 935 cm^{-1} to $^6A_{1g}(^6S) \rightarrow {}^4E_g(^4D)$ and that at 24 380 cm^{-1} to $^6A_1(^6S) \rightarrow {}^4T_1(^4D)$ is that the lower-energy transition has a considerably narrower linewidth than the transition at 24 380 cm^{-1} This is in accordance with the lower-energy transition occurring between states of the same orbital electronic configuration; of the excited states $^4E_g(^4D)$ and $^4T_2(^4D)$, only the former fulfills this condition. The transitions at 25 460 and 26 970 cm^{-1} are assigned, using Fig. 12, to $^6A_1(^6S) \rightarrow {}^4E(^4D)$ and $^6A_1(^6S) \rightarrow {}^4T_1(^4P)$, respectively. It can be seen that an acceptable set of assignments can be made for YIG and Fe^{3+}-doped $Y_3Ga_5O_{12}$ without recourse to lower-symmetry fields. However, we have mentioned that some of the lower-energy bands can be seen to be multicomponent. Under $\bar{4}$ and $\bar{3}$, T states reduce to an E and an A state, the former of which is doubly degenerate with respect to time-reversal symmetry. Hence, in YIG, which is a ferrimagnet, the E state should split into two components. We have observed three components in $^6A_{1g}(^6S) \rightarrow {}^4T_{1g}(^4G)$ at 77 K (Fig. 3) and in

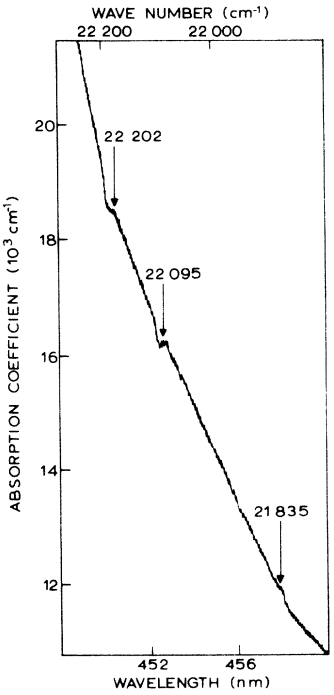

FIG. 13. Antiresonancelike fine structure on the broad vibronic band of $^6A_{1g}(^6S) \rightarrow {}^4T_{2g}(^4D)$ in $Y_3Fe_5O_{12}$ at 4.2 K.

TABLE VI. Energy separations of fine structure from $^4A_1(^6S) \rightarrow {}^4A_1(^4G)$ at 20 773 $cm^{-1} \pm 4$ cm^{-1} and from $^6A_{1g}(^6S) \rightarrow {}^4A_{1g}(^4G)$ at 21 450 ± 4 cm^{-1}.

Sideband energy from $^6A_{1g}(^6S) \rightarrow {}^4A_{1g}(^4G)$ (cm^{-1})		Sideband energy from $^6A_1(^6S) \rightarrow {}^4A_1(^4G)$ (cm^{-1})	
(i)	336 ± 29	(vi)	−427 ± 24
(ii)	385 ± 13	(vii)	337 ± 13
(iii)	480 ± 13	(viii)	732 ± 29
(iv)	645 ± 13		
(v)	752 ± 14		

$^6A_1(^6S) \rightarrow {}^4T_2(^4G)$ at 4.2 K.

VI. FINE STRUCTURE

The weak structure, some of which is shown in Figs. 5 and 13, is clearly not described by conventional absorption peaks. The two features at 22 095 and 22 202 cm^{-1} resemble inverted peaks and that at 21 110 cm^{-1} appears to consist of a mixture between an inverted peak and a dispersive line shape. The other features listed in Table V, although detectable, were not well enough resolved to be classified into line-shape types and are not shown. Previous observations of such phenomena[25,26] have been shown to arise when a narrow absorption impurity line overlaps a broad, continuous vibronic band.

We cannot account for these eight features in the YIG spectrum in terms of possible narrow transitions of the known impurities. Krebs and Maisch[34] have reported that for Fe^3 in Al_2O_3, there are exchange effects associated with the $^6A_{1g}(^6S) \rightarrow {}^4E_g$, $^4A_{1g}(^4G)$ transitions. Magnon sidebands could therefore be expected in YIG associated with these transitions. We have also observed sidebands on the high-energy side of the $^4E_g(^4G)$ state in $FeBO_3$ at 77 K which correspond to phonon energies observed in the Raman and infrared spectra. If we take the components at 20 773 and 21 450 cm^{-1} as band origins for these sidebands in YIG, one obtains the energy separations listed in Table VI. Table VII lists the spin-wave energies calculated by Douglass for YIG[38] and since the spin waves close to the Brillouin-zone edge are the most effective in producing sidebands,[39] we have underlined these energies. Van der Ziel *et al.*[40] have observed magnon sidebands on the $^6A_{1g}(^6S) \rightarrow {}^4T_{1g}(^4G)$ transition in YIG, separated from the pure electronic line by 290 and 343 cm^{-1}. We also observe antiresonance-like lines at the latter energy separation (Table VI) and assign lines (i) and (vii) of Table VI to a sideband involving the spin wave labeled k in Table VII. Table VII predicts no spin-wave energies much above 500 cm^{-1} and, therefore, we look to phonons as the source of the sidebands separated

TABLE VII. Spin-wave energies in YIG from Ref. 38.

n_0	n_c	Label	E (cm^{-1})
1	0	a	0
1	0	b	242
1	0	c	61
2	6	d	166
3	0	e	272
2	0	f	379
1	0	g	282
3	2	h	505
3	0	i	298
3	0	j	67
0	6	k	341
0	6	e	215

by 645 and 725 cm^{-1} [lines (iv), (v), and (viii) of Table VI] from the origins. Figures 14(a) and 14(b), showing the infrared absorption spectra of two thin sections of YIG at 300 K, indicate that there are absorption bands at 750, 650, and 420 cm^{-1}, which energies correlate well with separations (v), (viii), (iv), and (vi) of Table VI. The separation of -427 cm^{-1} then corresponds to the absorption of a phonon of this energy. The origin of the structure with energy spacings of 385 and 480 cm^{-1} is not clear but may correspond to spin-wave sidebands f and h of Table VII. If these assignments are correct, then we believe that this is the first observation of antiresonance lines caused by the interaction of a sideband with a vibronic continuum.

VII. INTENSITIES

The oscillator strengths of the best resolved transitions in YIG, $Y_3Fe_{0.29}Ga_{4.71}O_{12}$, and $Y_3Fe_{0.09}Ga_{4.91}O_{12}$ at 77 K were calculated using Eq. (3), where 2Γ (cm^{-1}) is the full width at half-height, N the density of absorbing centres, and $9/(n^2+2)^2$ is the Lorenz-Lorentz correction:

$$f=\frac{\Gamma\alpha_{\max}mc^2}{Ne^2}\,\frac{9n}{(n^2+2)^2}\,. \tag{3}$$

Transition heights and widths were taken from Gaussian fitting and the Lorenz-Lorentz correction applied for YIG and the dilute garnets using the refractive index data of Tables II and III. Table VIII lists the oscillator strengths for the transition in YIG at 77 K. Estimation of the oscillator strengths in the dilute garnet is complicated by the fact that Fe^{3+} has a site preference when doped into $Y_3Ga_5O_{12}$.[41,42]. We have used the data of Czerlinksy[42] to obtain estimates of the distribution of Fe^{3+} between tetrahedral and octahedral sites in $Y_3Ga_5O_{12}:Fe^{3+}$. Table IX lists the oscillator strengths so calculated.

The following information may be obtained from Tables VIII and IX: (a) The bands which do not fit into the crystal-field scheme are between one and two magnitudes stronger than the crystal-field transitions. (b) The oscillator strengths of several transitions which could be resolved in dilute and concentrated iron garnets were not independent of concentration, the intensities varying *approximately* as the square of the Fe^{3+} concentration. (c) The $^6A_{1g}(^6S)\rightarrow{}^4T_{1g}(^4G)$ transition increases its strength from 77 to 300 K.

These facts, together with the observation that, independent of Fe^{3+} site dilution (octahedral or tetrahedral), all bands in iron garnets reduce their intensity,[8] suggest that Fe^{3+}-Fe^{3+} interactions strongly influence the spectrum. Wood and Remeika[11] have studied the variation of band maxima with Fe^{3+} concentration for $^6A_{1g}(^6S)\rightarrow{}^4T_{1g}(^4G)$ and $^6A_1(^6S)\rightarrow{}^4T_1(^4G)$, observing that the intensities varied approximately as the square of the Fe^{3+} concentration.

As an aid to understanding the above phenomena, it is worthwhile to consider the mechanisms which have been invoked to explain the intensity of these crystal-field bands which for an isolated Fe^{3+} ion are doubly forbidden. Clogston[43] considered some

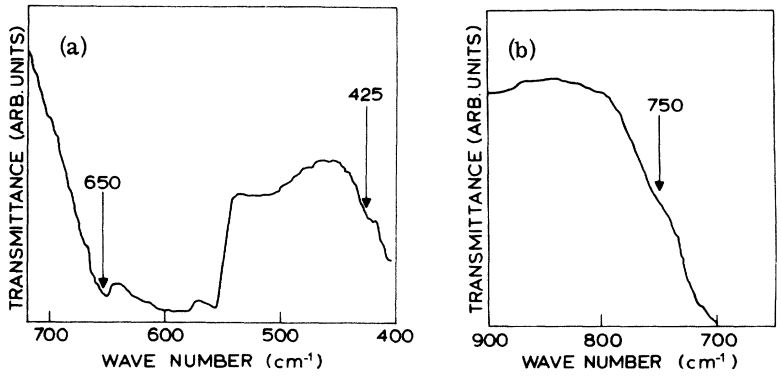

FIG. 14. Detail of the infrared absorption spectrum of YIG at 300 K on samples of thickness (a) 2.1 μm and (b) 18 μm showing absorption peaks at 650, 424, and 750 cm^{-1}.

TABLE VIII. Oscillator strengths of transitions in YIG at 77 K.

Transition energy (cm^{-1})	Assignment	Site	Oscillator strength
11 070	$^6A_{1g}(^6S) \rightarrow {}^4T_{1g}(^4G)$	oct	2×10^{-5}
14 550	$^6A_{1g}(^6S) \rightarrow {}^4T_{2g}(^4G)$	oct	2×10^{-5}
16 120 } 16 890 }	$^6A_1(^6S) \rightarrow {}^4T_1(^4G)$	tet	8×10^{-5}
19 718	$^6A_1(^6S) \rightarrow {}^4T_2(^4G)$	tet	1.6×10^{-4}
20 710	$^6A_1(^6S) \rightarrow {}^4E, {}^4A_1(^4G)$	tet	3.2×10^{-5}
21 390	$^6A_{1g}(^6S) \rightarrow {}^4E_g, {}^4A_{1g}(^4G)$	oct	2×10^{-5}
22 520	$^6A_{1g}(^6S) \rightarrow {}^4T_{2g}(^4D)$	oct	1×10^{-4}
23 110	Not crystal field, no assignment	oct/tet	2.6×10^{-3}/ 1.8×10^{-3}
24 150	$^6A_1(^6S) \rightarrow {}^4T_2(^4D)$	tet	6×10^{-5}
25 600	Not crystal field, no assignment	oct/tet	4.6×10^{-3}/ 3.1×10^{-3}
27 400	Not crystal field, no assignment	oct/tet	1.1×10^{-2}/ 7.6×10^{-3}

mechanisms whereby the $^6A_{1g}(^6S) \rightarrow {}^4T_{1g}(^4G)$ transition in YIG may gain intensity. The parity selection rule is relaxed by odd-parity phonons and spin-orbit interation mixes the $^6A_{1g}$ and $^4T_{1g}$ levels thus relaxing the spin selection rule. This explanation is consistent with the temperature dependence of this band and also with our observation that the magnetic circular dichroism of this band consists of two clear paramagnetic contributions centered at the energies of the two lower-energy components of $^6A_{1g}(^6S) \rightarrow {}^4T_{1g}(^4G)$ shown in Fig. 3. That the magnetic circular dichroism is of this form indicates that the Fe^{3+} ground state in the crystal is not pure $^6A_1$ but contains some orbital moment,[44] in agreement with Clogston's mechanism. Although the presence of some $^4T_1$ wavefunction in the ground state will relax the spin selection rule to the other quartet levels, some other mechanism must be invoked to explain the concentration dependence of the oscillator strengths of the crystal-

TABLE IX. Oscillator strengths for several transitions in YIG and $Y_3Ga_5O_{12}:Fe^{3+}$ (YGG : Fe^{3+}) at 77 K (from Ref. 42, Fe^{3+} concentrations in YGG : Fe^{3+} are Fe^{3+}(oct) = 0.223, Fe^{3+}(tet) = 0.067, $x = 0.29$; Fe^{3+}(oct) = 0.08, Fe^{3+}(tet) = 0.01, $x = 0.09$).

Crystal	Transition energy (cm^{-1})	Assignment	Site	Oscillator strength
YIG				2×10^{-5}
YIG				2.2×10^{-5}, 300 K
YIG	11 070	$^6A_{1g}(^6S) \rightarrow {}^4T_{1g}(^4G)$	oct	3×10^{-5} [a]
YGG : Fe^{3+}, $x = 0.29$				6×10^{-7}
YGG : Fe^{3+}, $x = 0.09$				3.5×10^{-7}
YIG				1×10^{-4}
YGG : Fe^{3+}, $x = 0.29$	22 600	$^6A_{1g}(^6S) \rightarrow {}^4T_{1g}(^4D)$	oct	5×10^{-7}
YGG : Fe^{3+}, $x = 0.09$				3×10^{-7}
YIG		No assignment,	oct/tet	$2.6\times10^{-3}/1.8\times10^{-3}$
YGG : Fe^{3+}, $x = 0.29$	23 110	not crystal field	oct/tet	$5.9\times10^{-5}/1.9\times10^{-4}$
YGG : Fe^{3+}, $x = 0.09$		transition	oct/tet	$2.6\times10^{-5}/2.1\times10^{-4}$
YIG		No assignment,	oct/tet	$4.6\times10^{-3}/3.1\times10^{-3}$
YGG : Fe^{3+}, $x = 0.29$	25 600	not crystal field	oct/tet	$1.7\times10^{-4}/6\times10^{-4}$
YGG : Fe^{3+}, $x = 0.09$		transition	oct/tet	$3.6\times10^{-5}/2.9\times10^{-4}$

[a] Ref. 11, 300 K.

field bands. To date, considerable work has been performed on these bands in Mn^{2+} compounds and it has been shown[45] that a large proportion of the intensity of these bands is due to exciton-magnon transitions, i.e., excitation of the crystal-field exciton on one sublattice a magnon on the other. Such a transition requires the presence of a neighboring ion coupled via superexchange, which is the situation in the iron garnets where there is a strong superexchange force between tetrahedral and octahedral sublattices and weaker antiferromagnetic interaction between each sublattice. The fact that dilution of either sublattice reduces the intensities of all such bands suggests that the magnons are created on one sublattice the excitons on the other. Dilution of tetrahedral Fe^{3+} will reduce (a) the intensities of the bands with excitons on the tetrahedral sites by dilution alone and (b) the intensities of bands with excitons on the octahedral sublattice by removing tetrahedral Fe^{3+} ions which, being coupled to octahedral Fe^{3+} via superexchange, allow the magnons to be excited. A similar argument follows for dilution of octahedral Fe^{3+}.

As to the origins of the stronger bands at 21 640, 23 110, 25 600, 27 400, and 29 000 cm^{-1} we suggest that they may arise from excitation of double excitons, i.e., transitions where two Fe^{3+} ions on the same sublattice or different sublattice are simultaneously excited to the spin quartet levels, e.g., ${}^6A_{1g}({}^6S) \rightarrow {}^4T_{1g}({}^4G) + {}^6A_{1g}({}^6S) \rightarrow {}^4T_{1g}({}^4G)$. From analogous phenomena in Mn^{2+} compounds[46] we expect these transitions to occur at the sums of the energies of the two transitions involved and to have oscillator strengths many times above those of the single-exciton (magnon assisted) bands. Such a description would account for the following facts: (i) These bands do not occur below 21 000 cm^{-1}. (ii) Those which can be studied with varying Fe^{3+} concentration have concentration-dependent oscillator strengths. (iii) The oscillator strengths are much larger than those of the single excitons.

Taking sums of transition energies in YIG from Table V we see from Table X that there is reasonable agreement with the energies of the observed bands. The considerable widths of these bands arise from the fact that the transitions of which they are sums are also broad. This double-exciton description is also consistent with the fact that the 27 400 cm^{-1} band is not seen in $Y_3Fe_{0.09}Ga_{4.91}O_{12}$ (Sec. IV). Unlike the other double-exciton bands listed in Table X, this one involves tetrahedral Fe^{3+}, and since the Fe^{3+} ion has a strong octahedral site preference in dilute garnets it is not surprising that this band is not seen in $Y_3Fe_{0.09}Ga_{4.91}O_{12}$. Most of the double-exciton energies listed in Table X involve only octahedral Fe^{3+} ions which have a weak antiferromagnetic interaction. It is not clear what role the ion on the tetrahedral site plays in modifying this interaction but that it does is witnessed by the effects of Ga substitution on the YIG spectrum.[8] Finally, it should be stated that previous assignments of some of these bands to charge-transfer transitions between O^{2-} and Fe^{3+} is also inconsistent with the spectra recorded from $Y_3Ga_5O_{12}:Fe^{3+}$ up to 45 000 cm^{-1}.[24]

VII. CONCLUSIONS

We have shown that the spectra of YIG and Fe^{3+}-doped $Y_3Ga_5O_{12}$ consist of (i) a series of Fe^{3+} crystal-field transitions originating from Fe^{3+} in octahedral and tetrahedral configurations and (ii) several much more intense transitions starting above 20 000 cm^{-1}. Assignments of the crystal-field transitions were made on the basis of band shapes, fine structure, and band energies in conjunction with the results of Gaussian fitting and a crystal-field calculation. Although the crystal-field calculation relied heavily on the correct assignment of the lower-energy transitions, in particular ${}^6A_{1g}({}^6S) \rightarrow {}^4E_g, {}^4A_{1g}({}^4G)$ and ${}^6A_1({}^6S) \rightarrow {}^4E_1, {}^4A_1({}^4G)$, to obtain the energies of the higher excited states, we found that reversal of the assignments of the abovementioned transitions gave the same assignments for the higher-energy transitions.

Fine structure observed on the vibronic envelope of several crystal-field transitions at 4.2 K in YIG have line shapes similar to those reported by Sturge *et al.*,[25,26] where interference occurs between weak narrow transitions on a broad continuum of absorption. We have assigned these lines to magnon and phonon sidebands of two crystal-field transitions.

The oscillator strengths of several transitions in the series of iron garnets $Y_3Fe_xGa_{5-x}O_{12}$ have been obtained and all exhibit an approximately linear dependence on Fe^{3+} concentration. We have suggested that for the crystal-field bands, the ex-

TABLE X. Probable double-exciton energies in YIG compared with band energies from Gaussian fitting to YIG and YGG: Fe^{3+} spectra.

Double-exciton energy (cm^{-1})		Energies of observed bands	2Γ (cm^{-1})
20 800 22 000 23 200	${}^4T_{1g}({}^4G) + {}^4T_{1g}({}^4G)$	21 640 23 110	1000 1800
24 950 25 550 26 150	${}^4T_{1g}({}^4G) + {}^4T_{2g}({}^4G)$ mean energy 25 600	25 600	2700
26 520 27 290 27 120 27 890 27 720 28 490	${}^4T_{1g}({}^4G) + {}^4T_1({}^4G)$	27 400	2500
29 100	${}^4T_{2g}({}^4G) + {}^4T_{2g}({}^4G)$	29 000	2200

citon-magnon transitions contribute considerable intensity and this allows an explanation of the origin of the concentration dependence of the oscillator strengths. For the more intense transitions we suggest that they arise from simultaneous excitation of two Fe^{3+} ions into the upper spin quartet levels and we demonstrate reasonable agreement between observed energies of these bands and where they would be expected. This interpretation is also consistent with the strength and concentration dependence of the strength of these bands.

The detection of the three intense transitions in the iron garnets around 23 200, 25 600, and 27 400 cm^{-1} is of particular relevance to the origin of the large increase in Faraday rotation observed when bismuth is substituted into YIG. It is known[20,21] that the transition or transitions giving rise to these large contributions to the Faraday spectrum occur around 24 500 cm^{-1}. In addition, to be able to explain the size of the rotation caused by the bismuth, commensurate with reasonable transition splittings, the oscillator strengths of such transitions must be of order 10^{-2}. These results imply not only that the crystal-field transitions are not responsible, but that the three intense transitions at 23 200, 25 600, and 27 400 cm^{-1} are probably involved in the enhancement of the Faraday rotation.

Clearly there remains much to be done in obtaining a fuller understanding of the YIG spectrum. Several lines of approach which might be fruitful are listed: (a) Temperature dependence of the crystal field transitions $^6A_{1g}(^6S) \rightarrow {}^4T_{1g}(^4G)$ as a guide to (i) whether the octahedral Fe^{3+} transitions are vibrationally assisted and if so the energies of the modes involved, and (ii) understanding of the role of superexchange in the crystal-field transitions; (b) Classification of the origin of fine structure around $^6A_{1g}(^6S) \rightarrow {}^4A_{1g}(^4G)$ and $^6A_1(^6S) \rightarrow {}^4A_1(^4G)$, (we suggest that a careful search around these transitions in $Y_3Ga_5O_{12}:Fe^{3+}$ will reveal exchange effects); (c) A more detailed study of the concentration dependence of oscillator strengths.

ACKNOWLEDGMENTS

We are pleased to acknowledge fruitful discussions with R. F. Pearson, H. I. Ralph, and G. Simpson and would like to express our gratitude to J. M. Robinson for all our crystal polishing, in particular, for the preparation of very thin samples, without which this work would have been severely curtailed. The supply of refractive-index data and technical assistance by J. Hewett, the writing and running of the fitting program by J. Morice, and chemical analysis by members of the analytical department are gratefully acknowledged. Thanks are also due P. Day of Oxford University for the use of his low-temperature spectrophotometer.

[1]J. Ferguson, Prog. Inorg. Chem. 12, 159 (1970), and references therein.
[2]D. S. McClure, *Electronic Spectra of Molecules and Ions in Crystals* (Academic, New York, 1959), and references therein.
[3]A. B. P. Lever, *Inorganic Electronic Spectroscopy* (Elsevier, New York, 1968).
[4]A. J. Kurtzig and H. J. Guggenheim, Appl. Phys. Lett. 16, 43 (1970).
[5]D. L. Wood, J. P. Remeika, and E. D. Kolb, J. Appl. Phys. 41, 5315 (1970).
[6]L. F. Mattheiss, Phys. Rev. B 2, 3918 (1970); 5, 290 (1972).
[7]R. G. Shulman and S. Sugano, Phys. Rev. Lett. 7, 157 (1961).
[8]S. H. Wemple, Surf. Sci. 37, 297 (1973); S. H. Wemple, S. L. Blank, J. A. Seman, and W. A. Biolsi, Phys. Rev. B 9, 2134 (1974).
[9]J. F. Dillon, J. Phys. Rad. 20, 374 (1959).
[10]K. A. Wickersheim and R. A. Lefever, J. Chem. Phys. 36, 844 (1962).
[11]D. L. Wood and J. P. Remeika, J. Appl. Phys. 38, 1038 (1967).
[12]K. W. Blazey, in Proceedings of the 18th Conference on Magnetism and Magnetic Materials, p. 735, 1972 (unpublished).
[13]S. L. Blank and J. W. Nielsen, J. Cryst. Growth 17, 302 (1972).
[14]A. I. Braginsky, T. R. Oeffinger, and W. J. Takei, Mater. Res. Bull. 7, 627 (1972).
[15]R. Hiskes and R. A. Burmeister, Ref. 12, p. 304.
[16]P. M. Grant, Appl. Phys. Lett. 11, 166 (1967).
[17]F. J. Kahn, P. S. Pershan, and J. P. Remeika, Phys. Rev. 186, 891 (1969).
[18]R. Krishnan, H. Le Gall, and T. K. Vien, Phys. Status Solidi A 17, K65 (1973).
[19]W. Wettling, B. Andlauer, P. Koidl, J. Schneider, and W. Tolksdorf, Phys. Status Solidi B 59, 63 (1974).
[20]D. E. Lacklison, G. B. Scott, H. I. Ralph, and J. L. Page (unpublished).
[21]D. E. Lacklison, G. B. Scott, H. I. Ralph, and J. L. Page, IEEE Trans. Magn. 9, No. 3, 457 (1973).
[22]D. E. Lacklison, H. I. Ralph, and G. B. Scott, Solid State Commun. 10, 269 (1972).
[23]B. Johnson and A. K. Walton, Brit. J. Appl. Phys. 16, 475 (1965).
[24]D. E. Lacklison, G. B. Scott, and J. L. Page, Solid State Commun. 14, 861 (1974).
[25]M. D. Sturge, J. Chem. Phys. 51, 1254 (1969).
[26]M. D. Sturge, H. J. Guggenheim, and M. H. L. Pryce, Phys. Rev. B 2, 2459 (1970).
[27]M. A. Gilleo and S. Geller, Phys. Rev. 110, 73 (1958).
[28]L. E. Orgel, J. Chem. Phys. 23, 1004 (1955).
[29]L. E. Orgel, J. Chem. Phys. 23, 1824 (1955).
[30]S. Koide and M. H. L. Pryce, Philos. Mag. 3, 607 (1958).
[31]L. L. Lohr, J. Chem. Phys. 55, 27 (1971).
[32]J. W. Stout, J. Chem. Phys. 31, 709 (1959).
[33]R. Stevenson, Phys. Rev. 152, 531 (1966).
[34]J. J. Krebs and W. G. Maisch, Phys. Rev. B 4, 757 (1971).
[35]Y. Tanabe and S. Sugano, J. Phys. Soc. Jap. 9, 753

(1954).
[36]*Atomic Energy Levels*, edited by Moore, Natl. Bur. Stand. (U. S.) Circ. No. 467, p. 65 (U. S. GPO, Washington, D. C., 1952).
[37]B. J. Hathaway and D. G. Halah, J. Chem. Soc. 2, 2400 (1964).
[38]R. L. Douglass, Phys. Rev. 120, 1612 (1960).
[39]R. L. Greene, D. D. Sell, W. M. Yen, and A. L. Schawlow, Phys. Rev. Lett. 15, 656 (1965).
[40]J. P. Van der Ziel, J. F. Dillon, and J. P. Remeika, Ref. 12, p. 254.
[41]S. Geschwind, Phys. Rev. 121, 363 (1961).
[42]E. R. Czerlinsky, Phys. Status Solidi 34, 483 (1969).
[43]A. M. Clogston, J. Phys. Rad. 20, 151 (1959).
[44]W. A. Crossley, R. W. Cooper, J. L. Page, and R. P. van Stapele, Phys. Rev. 181, 896 (1969).
[45]T. Fujiwara, W. Gebhardt, K. Petanides, and Y. Tanabe, J. Phys. Soc. Jap. 33, 39 (1972).
[46]J. Ferguson, Aust. J. Chem. 28, 307 (1968).